# CFD Simulation of a Vertical Induced Static Flotation Vessel

D. Lee and A. A. Mohamad
GLR Solutions Ltd., Calgary, Canada
(403) 219-2210 , www.glrsolutions.com

## 1.0 Introduction:

A better understanding of the fluid dynamics within a separation vessel or tank can allow for identification of design flaws and potential solutions for optimization.

Gas flotation separators (IGF's and ISF's) are even more complex and it is difficult, if not impossible, to optimize design by construction and operation of equipment alone. An additional tool to assist in optimizing oil in water removal is to utilize Computational Fluid Dynamic (CFD) modeling tools to simulate flow and phase behavior within these vessels or tanks to rapidly evaluate performance at a much lower cost and less time. While use of CFD for modeling fluid dynamics is not new, the techniques and code developed by GLR Solutions uniquely allow for modeling of the complex multiphase (oil, water, solids, and gas) conditions within flotation processes. By numerically modeling the process, it is much easier to manipulate conditions (geometry, flow rates, inlet concentrations, droplet size, etc.) to determine their individual impact on performance for both existing equipment or to prove performance for any proposed modifications to vessels/tanks.

This paper presents one approach for CFD modeling of multi phase flow within a vertical Induced Static Flotation (ISF) vessel of a common design and identifies a number of design issues that negatively impact separation performance.

## 2.0 Approaches to CFD:

Physical processes within the flotation vessel are very complex. Therefore, many assumptions must be adopted in the deriving of the model equation and accuracy of the solution depends on the validity of those assumptions. In this case, it was assumed that the flow is incompressible and properties are constant. In addition, the gas bubbles and oil droplets are treated as spherical particles. The free surface is assumed to be stationary and flat.

This CFD model is based on Euler/Lagrange approach for time-dependent calculations of three-dimensional flow of water with macro gas bubbles and oil droplets. The water flow was calculated on the Euler approach by solving a three-dimensional Reynolds-averaged conservation equation (Navier Stokes equation) with a k-e turbulent model. Two-way coupling was accounted for by adding dispersed phase source terms in all conservation equations of the continuous phase. Gas bubble and oil droplet motion was calculated by

solving an equation of motion taking into account drag force, pressure, lift force and buoyancy.

For the case presented, the following inlet conditions were established and remained constant throughout:

Water Flow Rate = 600 $m^3$/hr
Oil in Water Concentration = 300 ppm
Oil Viscosity = 0.0531 N.s/$m^2$
Oil Specific Gravity =0.96
Oil Droplet Size = we examined from 3 μm to 200 μm
Water Temperature = 80 °C
Water density = 980 kg/$m^3$
Gas Volume Flow Rate= 0.032 $m^3$/s (68 cfm)
Gas Bubble Size = 150-300 μm
Gas Density =0.657 kg/$m^3$
Gas Viscosity =1.12x$10^{-5}$ kg/(m.s)

Figure 1 shows a schematic diagram of the vessel utilized for this particular model. The flow enters the vessel through a vertically oriented nozzle located at bottom. The resulting inlet water jet is confined within a vertically oriented cylindrical shell to prevent short circuits with the vertically oriented outlet at the bottom of the vessel. At the top of the vessel there is a skimming weir that runs the circumference which contains several outlet nozzles where skimmed oil can be taken out.

The physical dimensions of the vessel are 3.6 m diameter x 3.8 m height. The inlet and outlet nozzle diameter is 0.254 m (10 ). The jet confining cylinder dimension was 3.5 m in height and 3.05 m in diameter. Based on the flow conditions established, it was determined that there was approximately a 4 minute retention time across the vessel.

## 2.1 Basic Conservation Equations (Dispersed Phase):

The critical equations utilized within our model are defined below:

### 2.1.1 Momentum Equation:

The momentum equation for a droplet of mass $m_d$ is:

$$m_d \frac{du_d}{dt} = F_{dr} + F_p + F_{am} + F_b \quad (1)$$

$$F_{dr} = \frac{1}{2} C_d \rho A_d |u - u_d| (u - u_d) \quad (2)$$

$$F_p = -V_d \nabla P \quad (3)$$

$$F_{am} = -C_{am} \rho V_d \frac{d(u_d - u)}{dt} \quad (4)$$

$$F_b = m_d\left[g - \vec{\omega}\, X\, (\vec{\omega}\, X\, r) - 2(\vec{\omega}\, X\, u_d)\right] \quad (5)$$

$$\frac{d x_d}{dt} = u_d \quad (6)$$

$$\tau_M = \frac{m_d |u - u_d|}{|F_{dr}|} = \frac{2 m_d}{C_d \rho A_d |u - u_d|} = \frac{4 \rho_d D_d}{3 C_d \rho |u - u_d|} \quad (7)$$

### 2.1.2 Mass Equation:

$$\frac{d m_d}{dt} = -A_d F_m \quad (8)$$

$$F_m = K_g p_t \ln \frac{(p_t - p_{v,\infty})}{(p_t - p_{v,s})} \quad (9)$$

$$\tau_m = \frac{m_d}{A_s |F_m|} = \frac{\rho_d D_d}{6 |F_m|} = \frac{\rho_d D_d}{6 K_g p_t \ln \left| \frac{(p_t - p_{v,\infty})}{(p_t - p_{v,s})} \right|} \quad (10)$$

## 3.0 Simulation Results:

Figure 2 shows trajectories of gas bubbles and oil droplets. It is clear that the jet after issuing from the inlet nozzle expands and bubbles coalesce and disperse. The jet expansion is controlled by the confining cylinder. The presence of the confining cylinder is essential to prevent the gas bubbles and oil droplets direct flow to the outlet.

As the flow rises through the confining cylinder, we see fairly even flow velocities about 1 m from the jet inlet. However, we observe a preferential pathway for both gas bubbles and oil droplets along the interior wall of the confining cylinder. Yet we see the highest water velocities at the center of the confining cylinder.

As the water reaches the top of the confining cylinder, it is free to flow in both a horizontal and downward vertical axis. Since the outlet nozzle can not be at center of the vessel it has been placed off-center on one side. As a result we observe the flow becoming asymmetric and three dimensional.

Figure 3 shows velocity vectors at the mid-cross section of the vessel. There is evidence of a donut-type vortex formation around the inlet jet at the bottom of the vessel. A closer look at flow patterns on other sections of the vessel are shown in Fig. 4-6. The main reason for formation of the vortex is that the jet issues with high velocity and pressure decreases around the jet which results of flow toward the jet fluid entrainments.

Figures 7-9 show flow pattern at different horizontal sections. Figure 7 is a flow pattern at the bottom of the vessel. Figure 8 shows the velocity vectors at the section near the skimming outlets. Figure 9 shows velocity vectors at the section where the jet flow leaves

the confining cylinder. The flow becomes almost uniform about one meter after the jet inlet. In fact, when testing various inlet flow rates, it is found that as the flow rate decreases the flow becomes almost uniform after a short distance from the jet inlet. It is also observed that the confining cylinder enhances coalescence rates as the cylinder walls increase the probability of bubble collision and result in rapid growth in bubble size.

Figure 10 shows velocity vectors at the free surface of the vessel. The radial flow is clearly evident and we find the flow to be fairly symmetrical. However, the flow becomes asymmetric in the annular gap between the vessel and the jet confining cylinder because the off-set location of the outlet nozzle at the bottom of the tank.

The results of this simulation reflect the physics of flow under these specific conditions. It is worthy to mention that a simulation of water flow without gas bubbles and/or oil droplets is very different than the flow with gas bubbles and/or oil droplets. It is intended to say that it is not appropriate to extrapolate data or simulation results without gas bubbles for IGF/ISF simulation.

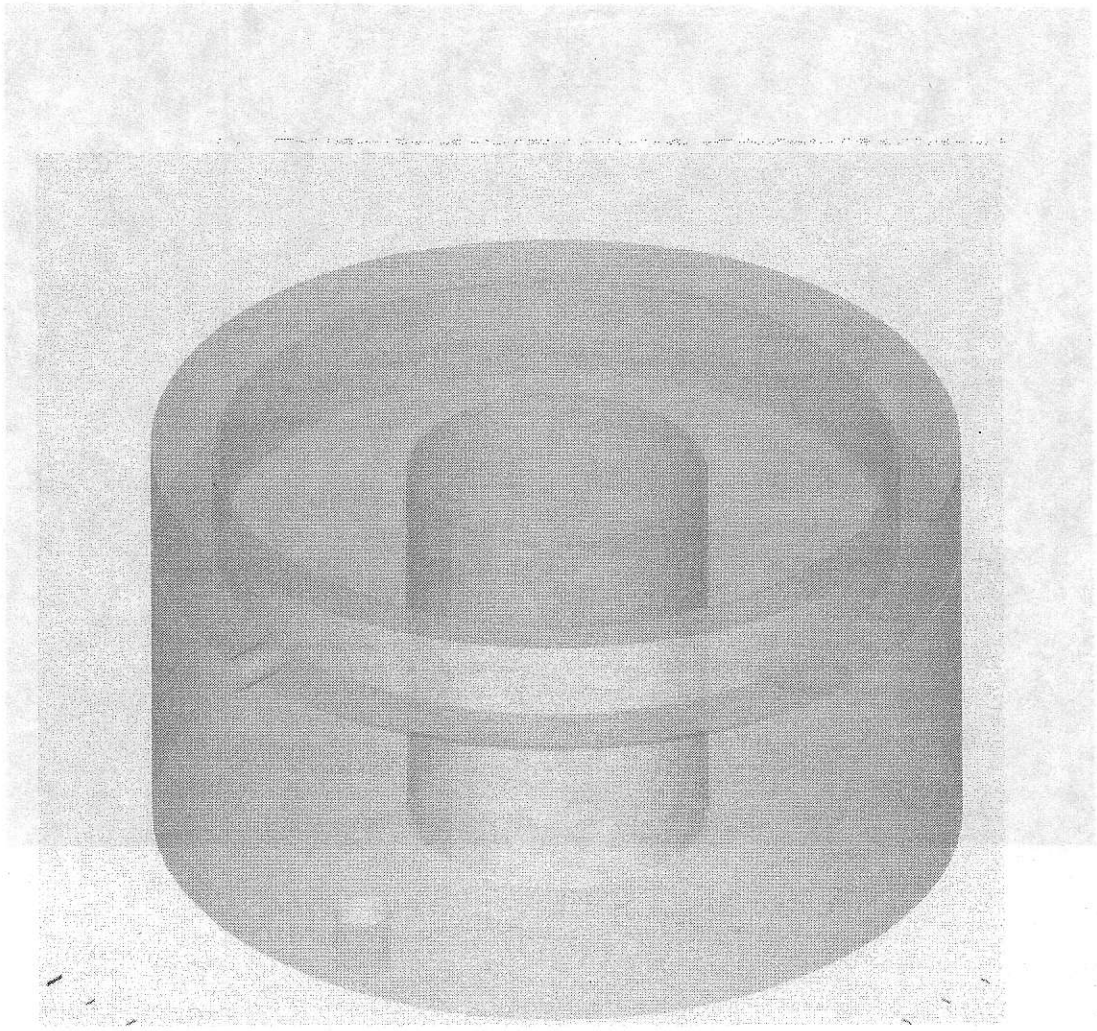

Fig. 1 Schematic diagram of the skim vessel.

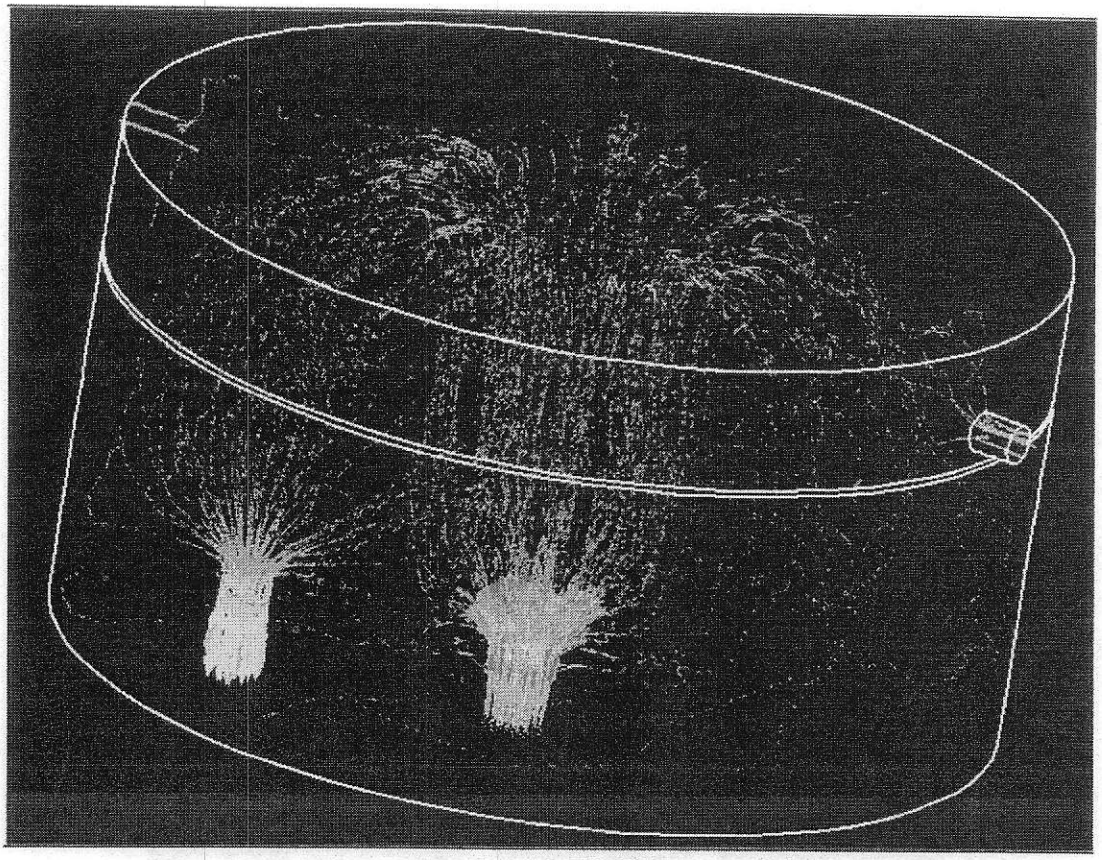

Fig. 2 Gas bubbles and oil droplets trajectories.

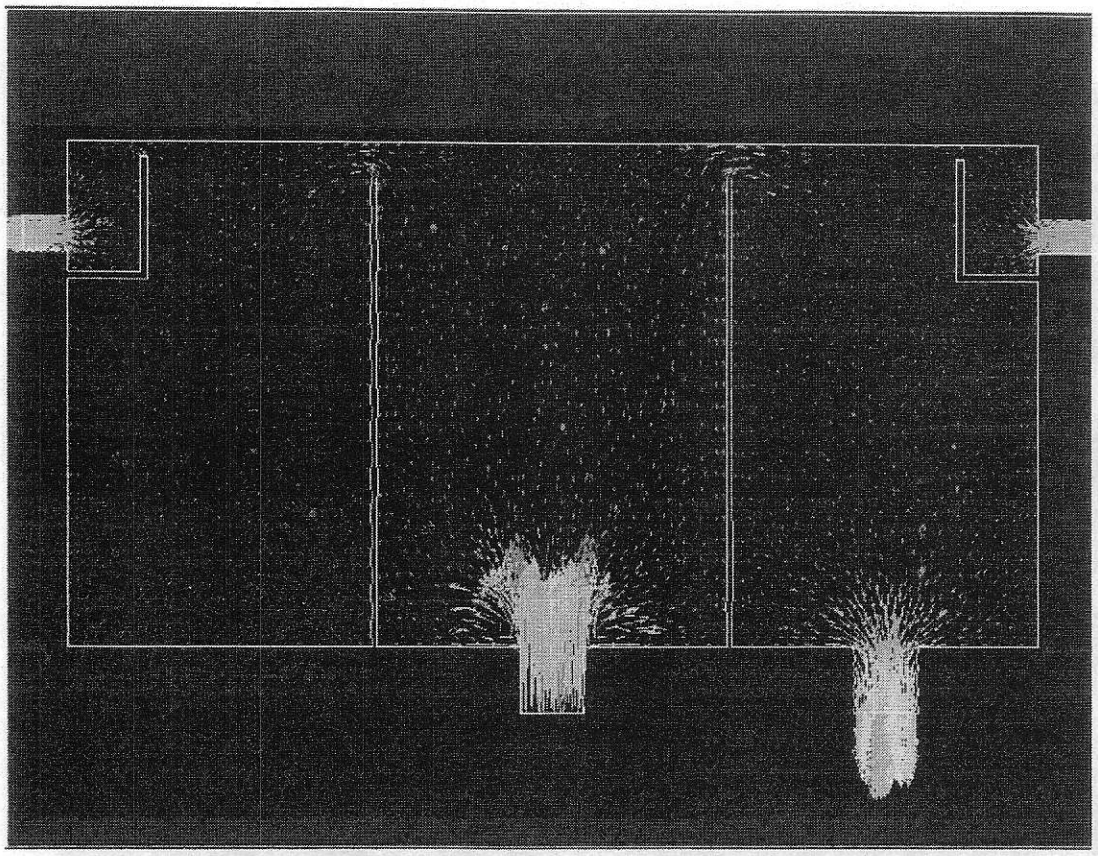

Fig. 3 Velocity vectors at mid-cross section of the vessel.

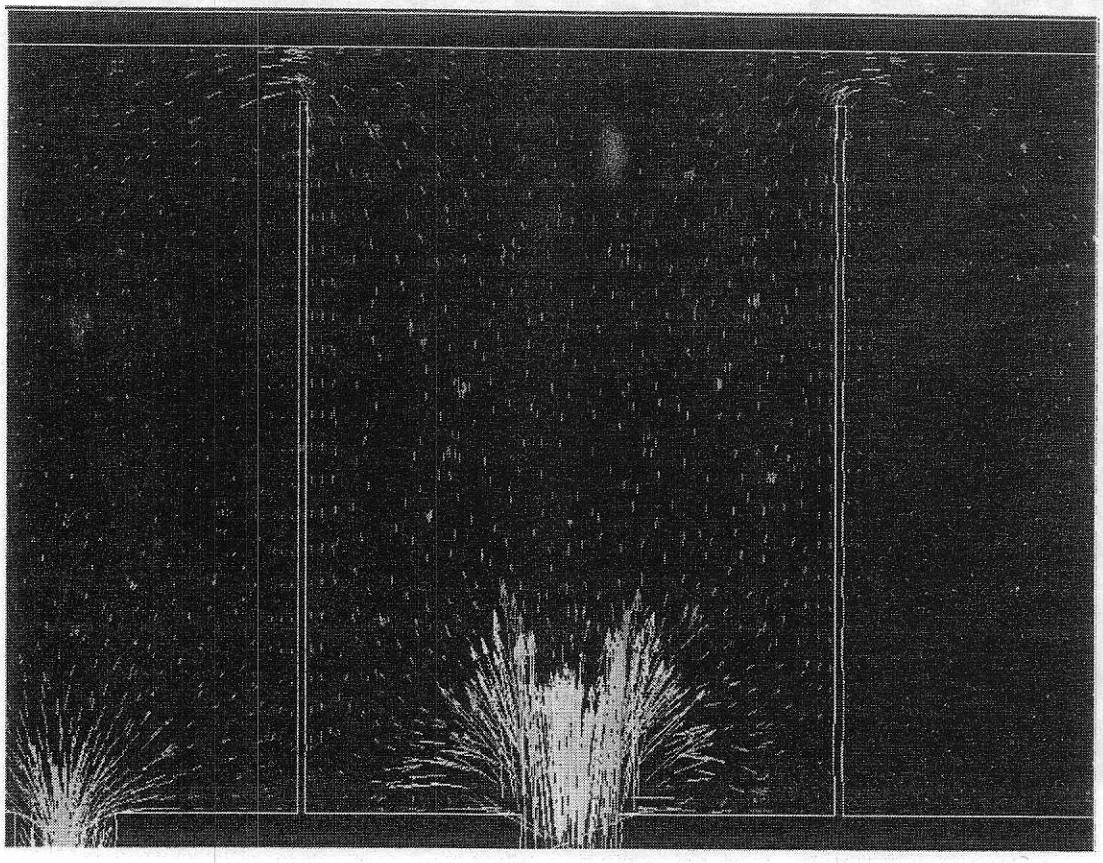

Fig. 4 Velocity vectors at the middle section of the vessel.

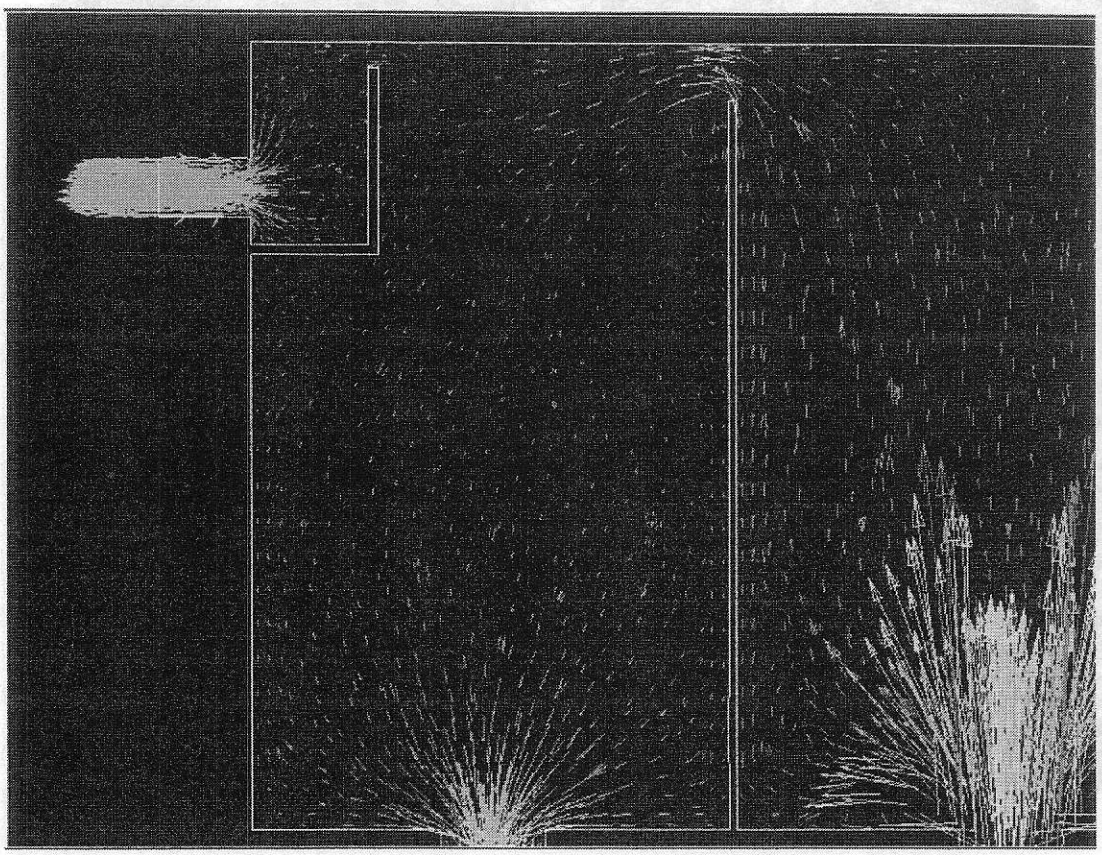

Fig. 5 Right-hand section of the vessel.

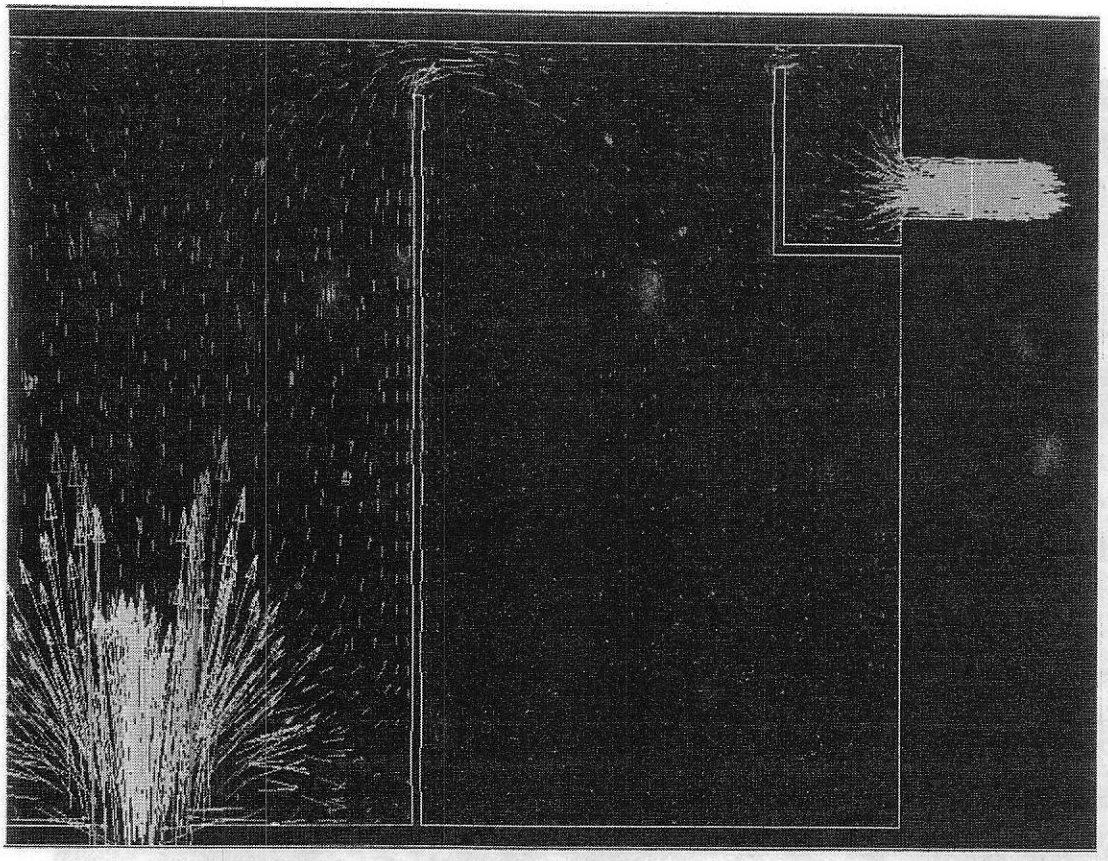

Fig. 6 Left-hand section of the vessel.

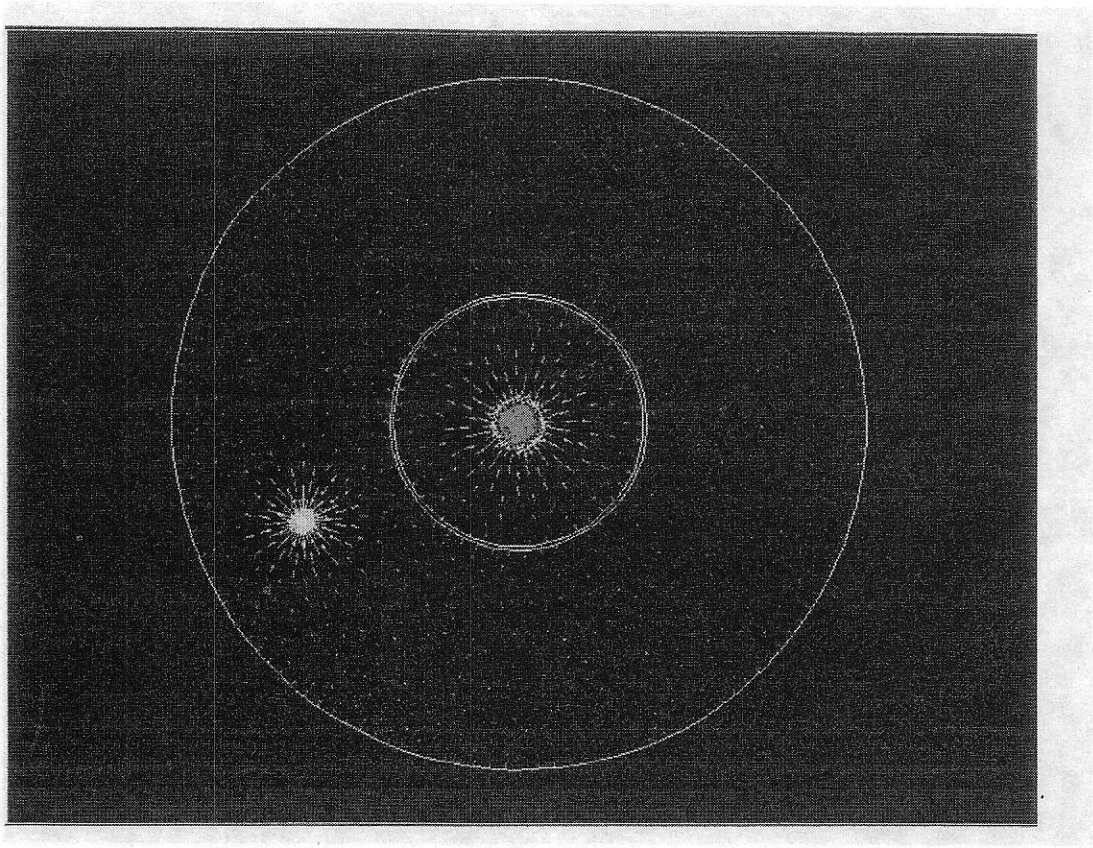

Fig. 7 Flow pattern at the bottom of the vessel near the inlet and outlet.

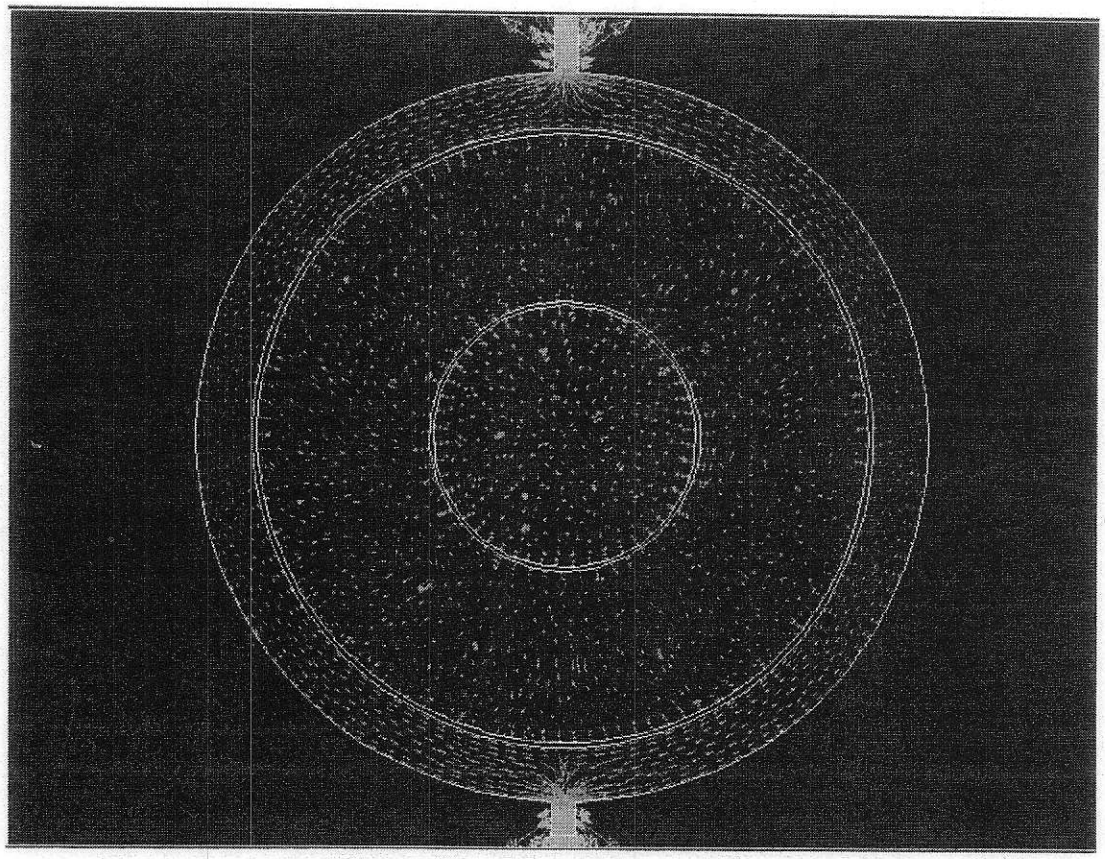

Fig. 8 Velocity vectors near the skimming outlets.

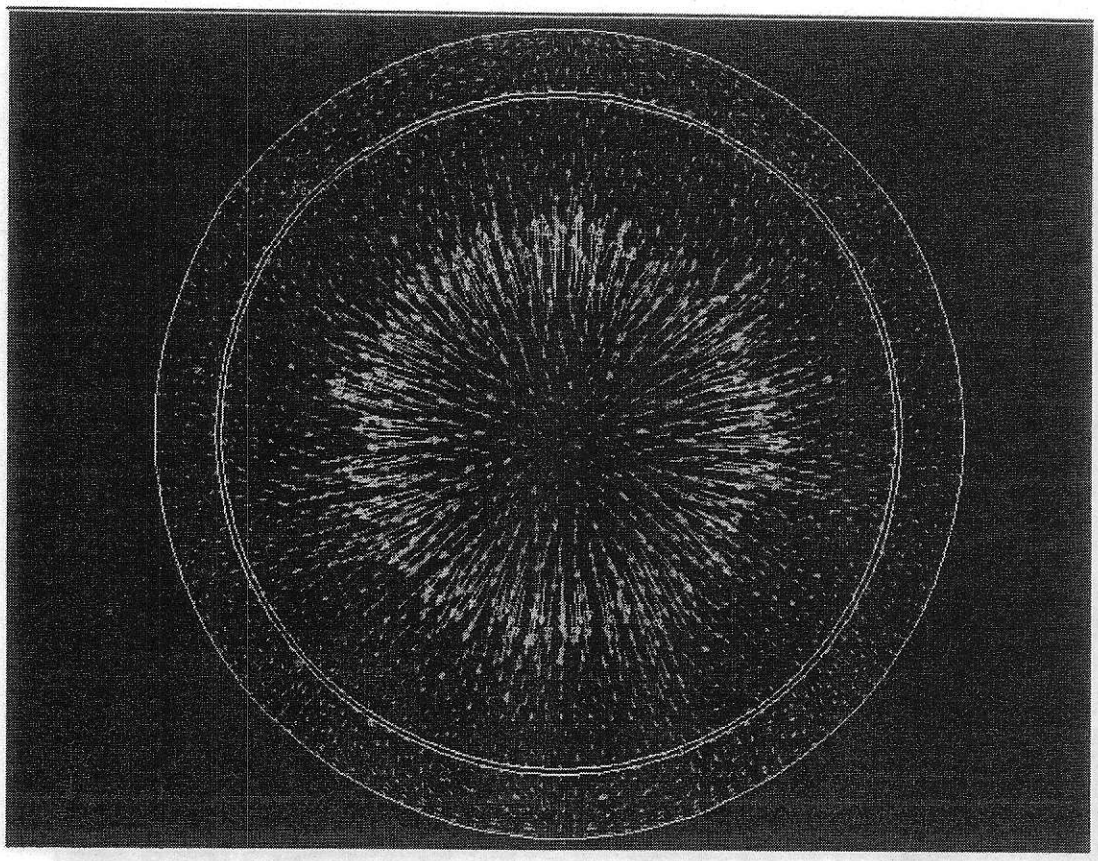

Fig. 9 Velocity vectors at section where the jet flow leaves the confining cylinder.

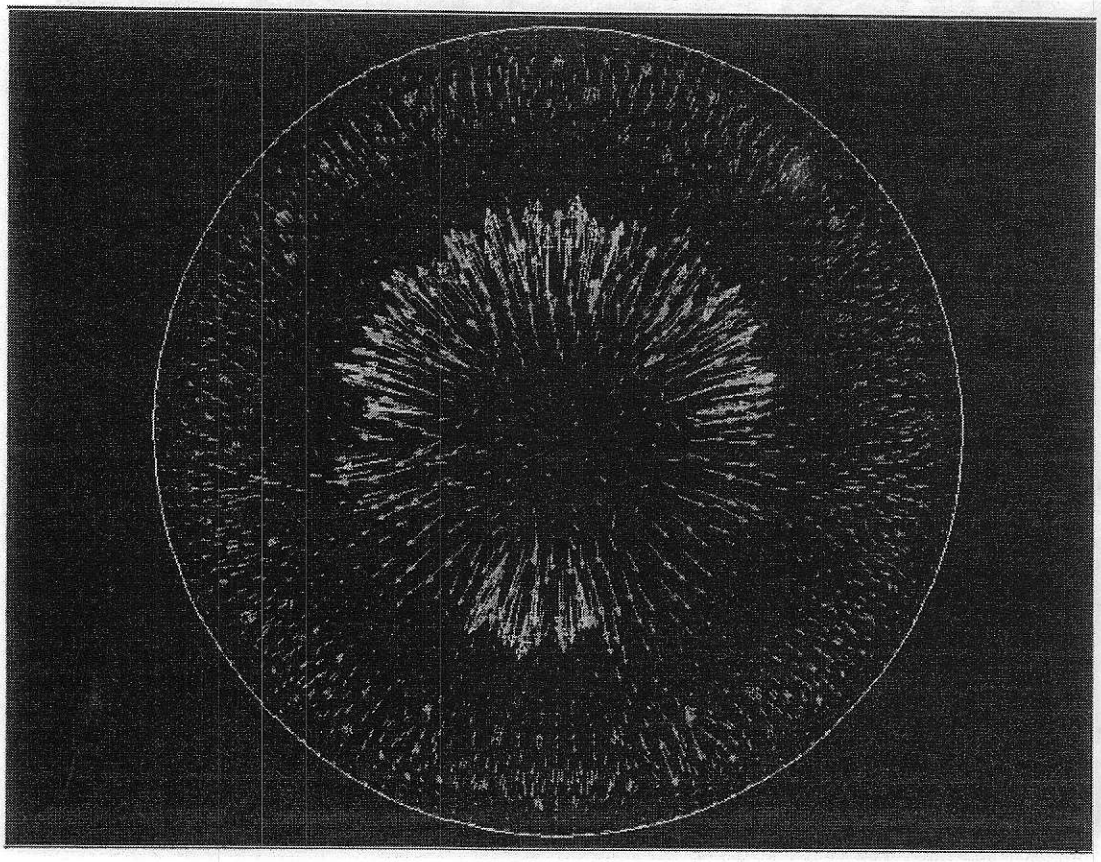

Fig. 10 Velocity vectors at the free surface of the vessel.

## 4.0 Conclusions:

The results of this simulation show that it is possible to investigate the effect of different controlling and operating parameters on the performance and efficiency of a separation vessel.

The physics of the flow is quite complicated; hence it is impossible to determine the precision of the resulting data in particular due to the number of modeling assumptions and difficulty in calculating the rate of coalescence. However, we feel confident that as a qualitative tool this is extremely useful for design and operation purposes.

The results clearly show the effectiveness of the jet confining cylinder for initial contact of gas and oil droplets while preventing short circuiting to the outlet. The results also indicate that the confining cylinder also acts to establish a desirable surface flow pattern for skimming of oil/froth. However, we see that the surface turbulence allows a significant amount of water over the skimming weirs when skimming is set up in a continuous operation. Therefore, it is advisable to operate this particular vessel geometry with a batched skimming philosophy at timed intervals to allow for oil accumulation. The model also shows that the walls of the confining cylinder act to rapidly coalesce inlet gas bubbles which has the impact of increasing their rise velocity and turbulence within the surrounding water. This is viewed as a negative design aspect given the reduced probability of oil-bubble attachment and ultimately lower oil removal efficiency.

Due to the design of this vessel, we observe a very limited window for contact of gas bubbles and oil droplets. When larger gas bubbles are entrained (>75 microns), essentially these two phases are only in intimate contact with each other during the period of retention within the confining cylinder. Once these large bubbles reach the surface they are released into the headspace and don't sink and there is no further contact or lift with the oil. The particle trajectories, observed in Figure 1, going down to the outlet are predominantly those of oil alone as these larger gas bubbles cannot sink at these water velocities. This is in contrast to much smaller bubbles (< 75 microns) when they are modeled which are able to descend for a short distance prior to fully coalescing and rising to the surface. These conclusions were impacted further by the walls of the confining cylinder which acts as a coalescing surface for the gas bubbles, i.e. rapidly exaggerating their size because they are trapped in that zone free to coalesce on those walls. While coalescing effect cannot be eliminated, the performance of oil removal can be improved by entraining smaller bubbles into the inlet stream so that a reasonable bubble size is maintained even after wall coalescing effects.

The off set designed location of the outlet nozzle on this vessel creates an asymmetric and three dimensional flow patterns. The result is a higher velocity vortex down one side of the vessel. We observe that smaller oil droplets are freely caught in this higher velocity zone and become free to leave in the outlet water. Better design can be achieved by replacing the single outlet of the vessel with multiple outlets evenly distributed at the

bottom. This conclusion becomes more significant as the droplet size of the oil and bubbles decreases.

As a summary, we find this CFD modeling gives clear insights of flow distribution which helps in better understanding optimal design and operation conditions for this particular vessel under these specific conditions. Our intent is not to criticize this design but rather to demonstrate the value of using CFD as a support to the engineering design process for complicated multi phase conditions.

The model developed is quite flexible and can simulate a wide range of inlet conditions and flow rates. We would like to point out that different inlet conditions may result in alternative conclusions.

**Nomenclature:**

| | |
|---|---|
| $A_d$ | cross-sectional area of the droplet |
| $A_s$ | droplet surface area |
| $C_d$ | drag coefficient |
| $C_{am}$ | virtual mass coefficient |
| $D_d$ | droplet diameter |
| $F_b$ | body force |
| $F_{dr}$ | drag force |
| $F_{am}$ | virtual mass force |
| $F_m$ | rate of mass transfer per unit surface area |
| $F_p$ | pressure force |
| $K_g$ | mass transfer coefficient |
| $m_d$ | mass of droplet |
| u | fluid velocity |
| $u_d$ | droplet velocity |
| $p_t$ | gas pressure |
| $p_{v,\infty}$ | partial pressure of vapor in the droplet surroundings |
| $p_{v,s}$ | partial pressure of vapor at its surface |
| r | distance vector to the axis of rotation |
| $T_d$ | droplet temperature |
| $V_d$ | droplet volume |
| $x_d$ | droplet position vector |

**Greek Symbols:**

| | |
|---|---|
| □ | gradient |
| $\rho_d$ | droplet density |
| $\vec{\omega}$ | angular velocity vector |
| $\tau_m$ | mass relaxation time scale |
| $\tau_M$ | momentum relaxation time scale |